Egyptian Journal of Chemistry

http://ejchem.journals.ekb.eg/

Synthesis, Structural Characterization, Thermal Behaviour and Antimicrobial Activity of Copper, Cadmium and Zinc Chelates of Traizole-thiole Ligand in Comparison with Theoretical Molecular Orbital Calculations

Hayam A. Abd El Salam*[1], Ehab M. Zayed[1], M. A. Zayed[2], Mahmoud Nouman[2]

[1]Department of Green Chemistry, National Research Centre (NRC), 33 EL-Bohouth Street (former EL-Tahrir Street), Dokki Giza Egypt, P.O.12622.
[2]Chemistry Department, Faculty of Science, University of Cairo, Giza, 12613, Egypt.
[3]Mathematics Department, Faculty of Science, University of Cairo, Giza, 12613, Egypt.

THIS research involved structural and molecular behaviour of the ligand HL, 4-amino-5-(2,2-dichloro-1-methylcyclopropyl)-4H-1,2,4-triazole-3-thiol toward the transition metal ions namely Cu (II), Cd(II) and Zn (II) had been studied using elemental analyses, magnetic, electronic, FT- IR, ^{1}H-NMR, XRD and Thermal analyses (TGA and DTA). The interpretation of practical data obtained had been evaluated and confirmed by theoretical molecular modelling. The computations had been done by software of Gaussian 09W package. The geometries of traizole-thiole ligand and its metal chelates were fully optimized using density functional theory B3LYP method. Their structures were confirmed via correlation between experimental and theoretical calculations. The ligand and its metal chelates biological activities had been tested against Gram-positive (*Staphylococcus aureus* ATTC 12600), Gram-negative (*Escherichia coli* ATTC 11775 and) bacteria, two fungus (*Aspergillus flavus* and *Candida albicans*).

Keywords: Traizole-Thiole, Metal-Chelates, Thermal- Spectroscopic analyses, XRD, Molecular orbital calculations, Biological activity.

Introduction

Traizole-Thiole derivatives are significant heterocyclic compounds. They were used in the preparation of antibiotics, fungicides, herbicides and plant growth hormone insulators [1]. They are considered good corrosion inhibitions [2]. Heterocyclic compounds containing Triazole-Thiol rings are very interesting due to their biological significant characters such as antiviral [3], analgesic, antimicrobial, anticonvulsant, anticancer, antioxidant, antitumor[4] and antidepressant effects[5]. The Triazole-Thiol derivatives are of diverse pharmacological

properties [6,7]. The inclusion of triazole ring to new drugs makes them therapeutically interesting molecules as previously reported [8,9]; as examples Vorozole, Letrozole and Anastrozole, had been used for the remedy of breast cancer [8, 9]. The presence of N and S atoms as coordination active sites in Traizole-Thiole derivatives leads to formation of numerous metallo-biomolecules of interesting biological activities [10, 11]. The complexation of drug to a metal ion promotes its activity and in some instances the complex has more biological activity than the corresponding drug [12]. The Traizole-Thiole ligands of N and S donor atoms in their structures are considered

good chelating agents for the transition and non-transition metal cations [13]. The Traizole-Thiole metal chelates are of great interest due to their contributions [14] and their potential uses in applied sciences [15-17]. Furthermore, metal chelates containing Triazole- ligands also show great biological activity [17]. In continuation to our previous work on metal chelates, the present study involved coordination behaviour of novel 4-amino-5-(2,2-dichloro-1-methylcyclopropyl)-4H-1,2,4-triazole-3-thiol [18] toward Cu (III), Cd (II) and Zn (II) and the structures of the studied HL ligand and its solid chelates are elucidated by experimental data which confirmed through TD-DFT approximations at the same level of theory. The biological activities of the prepared novel Traizole-Thiole and its metal chelates are reported and compared with standard antibiotic drugs as references [19].

Experimental

Materials and reagents

All chemicals used in this research are of highest purity available. They included Cu (II) chloride hex hydrate (Prolabo), Cd (II) and Zn (II) chloride (BDH). Organic solvents used included absolute ethyl alcohol and dimethylformamide (DMF). These spectroscopic pure solvents were purchased from BDH. De-ionized water collected from all glass equipments was used in all aqueous solutions preparations.

Instruments

Elemental microanalyses (C, H, N, and S) of the prepared novel ligand and its solid chelates had been performed in the Microanalytical centers at Cairo Universityusing CHNS-932 (LECO) Vario Elemental Analyzers. The accuracy of the data was checked by repeated readings twice. The Perkin-Elmer FT-IR type 1650 spectrophotometer was used to measure spectra in the region 4,000–400 cm^{-1} as KBr disks. The ^{1}H-NMR spectra were recorded with a JEOL EX-500 MHz in DMSO-d6 as solvent, where the chemical shifts were determined relative to the solvent peaks. The mass spectrum (MS) was recorded by the electron impact (EI) technique at 70 eV using MS-5988 GS-MS Hewlett-Packard instrument. The diffused reflectance spectra were measured on a Shimadzu3101 pc spectrophotometer. The molar magnetic susceptibility was measured on powdered samples using Faraday method. The diamagnetic corrections were made by Pascal's constant, and Hg[Co(SCN)4] was used as a calibrant. The magnetic data for the background of the sample holder were corrected. The molar conductance of solid chelates in DMF (10^{-3} M) was measured using Sybron-Barnstead conductometer (Meter-PM, E = 3,406). The thermal analyses

(TG, DTG and DTA) were carried out in dynamic nitrogen atmosphere (20 mL min^{-1}) with two heating rates of 10 ^{o}C and 20 ^{o}C min^{-1} using Shimadzu TG-60H thermal analyzer.

Synthesis of the ligand and its metal chelates
Synthesis of the triazole ligand

An equimolar amounts of 2,2-dichloro-1-methylcyclo propane carboxylic acid (1.67, 10 mmol) and thiocarbohydrazide (1.06 g, 10 mmol) were heated in an oil bath at 140 for 4 h. the completion of reaction was checked by TLC (pertrolium ether / ethyl acetate 3:1). The reaction mixture was cooled to room temperature and the excess of acid was removed by stirring the solid product with saturated solution of sodium bicarbonate. The insoluble solid product was then filtered, dried and recrystallized from methanol to give slightly yellow crystal. Yield 80%, m.p.=123 °C.

Synthesis of the metal chelates

The metal chelates were prepared by the addition of hot solution (60 ^{o}C) of the Cu, Cd and Zn chloride (0.1 mmol) in absolute ethanol (15 mL) to the hot solution (60 ^{o}C) of the triazole-thiole ligand (0.6 g, 0.219 mmol) in ethanol and DMF (15 mL). The resulting mixture was heated and left under reflux for four hours with stirring. The solvent was evaporated to get precipitate; which recrystallized from DMF. The crystalline precipitate was dried and weighed to calculate it's present yield.

Computational details

All computations were carried out using Gaussian 09W software package [20]. The molecular geometry for the studied compounds was fully optimized using density functional theory B3LYP method. Where (B3) [21-23] stands for Becke's three parameters exact exchange-functional combined with gradient-corrected correlation functional of Lee, Yang and Parr (LYP) [24]. DFT/GENECP level had been obtained by implementing Def2TZVP basis set for Fe, Co and Ni-atoms [25, 26] and 6-311++G(d,p) [27, 28] basis set for the rest of atoms. No symmetry constrains were applied during the geometry optimization [29, 30]. The choice of mixed basis set was due to flexibility, accuracy, consistent and better performance of the Alrich's effective core potentials basis set (def2-TZVP) with Gaussian type triple- ζ potential(6-311++G(d,p) [31]. By using HOMO and LUMO energy values for complexes, electronegativity and chemical hardness can be calculated as follows: X= (I + A)/2 (electronegativity), η=(I-A)/2 (chemical hardness), S = 1/2η (chemical softness) where I and A are ionization potential and electron affinity, and I= - EHOMO and A= - ELUMO,

respectively [32-34]. NBO calculations had been performed at the same level of calculation by using NBO 3.1 program as implemented in the Gaussian 09W software package. Throughout this work optimized structures were visualized using Chemcraft version 1.6 package [35] and Gauss View version 5.0.9 [36]. The first 15, 85, 65 and 65 low-lying excited states for ligand and Fe, Co and Ni complexes respectively had been calculated within the vertical linear-response TD-DFT approximation [37-41] at the same level of theory to calculate the electronic absorption spectra of thestudied compounds. The total static dipole moment (μ), the mean polarizability $<\alpha>$, the anisotropy of the polarizability and the mean first hyper-polarizability $<\beta>$ using the x, y, z components were calculated by using the following equations [42-44]:

$$\mu = (\mu_x{}^2 + \mu_y{}^2 + \mu_z{}^2)^{\frac{1}{2}}$$

$$\alpha = \frac{(\alpha_{xx} + \alpha_{yy} + \alpha_{zz})}{3}$$

$$\Delta\alpha = \sqrt{\left[\frac{(\alpha_{xx} - \alpha_{yy})^2 + (\alpha_{yy} - \alpha_{zz})^2 + (\alpha_{z\square} - \alpha_{xx})^2}{2}\right]}$$

$$\beta = \beta_x{}^2 + \beta_y{}^2 + \square_z{}^2 \text{, where}$$

$$\beta_x = \beta_{xxx} + \beta_{xy\square} + \beta_{xzz}$$

$$\beta_y = \beta_{yyy} + \beta_{xx\square} + \beta_{yzz}$$

$$\beta_z = \beta_{zzz} + \beta_{xx\square} + \beta_{yyz}$$

Biological activity

The test was done using the diffusion agar technique. Spore suspension (0.5 mL, 10-6–10-7 spore mL^{-1}) of each of the investigated organism was added to a sterile agar medium just before solidification, then poured into sterile Petri dishes (9 cm in diameter) and left to solidify. Using sterile cork borer (6 mm in diameter), three holes (wells) were made into each dish, and then 0.1 mL of the test compound dissolved in DMF (100 mg mL^{-1}) was poured into these holes. The dishes were incubated at 37 ºC for 48 h where clear or inhibition zones were detected around each hole. DMF (0.1 mL) was used as a control under the same conditions. By subtracting the diameter of the inhibition zone resulting with DMF from that obtained from each metal chelate or the free ligand, antimicrobial activities were calculated as a mean of three replicates (Ekennia et al., 2017)[45].

Results and Discussion

Structure characterization of ligand and its metal chelates

Traizole-Thiole ligand under investigation is characterized by elemental analysis (Table 1). It has molecular formula ($C_6H_8Cl_2N_4S$). It has mole mass of 239.13 mg mole^{-1}. Its structural formula is proposed depending upon FT-IR, ^{1}H-NMR and mass spectra measurements (Fig. 1).

Its metal chelates of Cu (II), Zn (II), and Cd (II), are obtained via the Traizole-Thiole ligand reaction with metal ions in ratio of 1: 2 (metal: ligand) as given by Scheme 1.

The Traizole-Thiole prepared ligand and its chelates are stable at 27^{0}C and are mostly soluble in DMF and DMSO. The (CHNS) elemental analyses data, melting points and yields of the studied compounds are represented in Table 1. The proposed structures of the studied chelates are compatible with the analytical data in Table 1. The melting point of ligand is found to be 120 ºC; while that of chelates are ranged from 100 to 289 ºC.
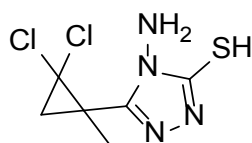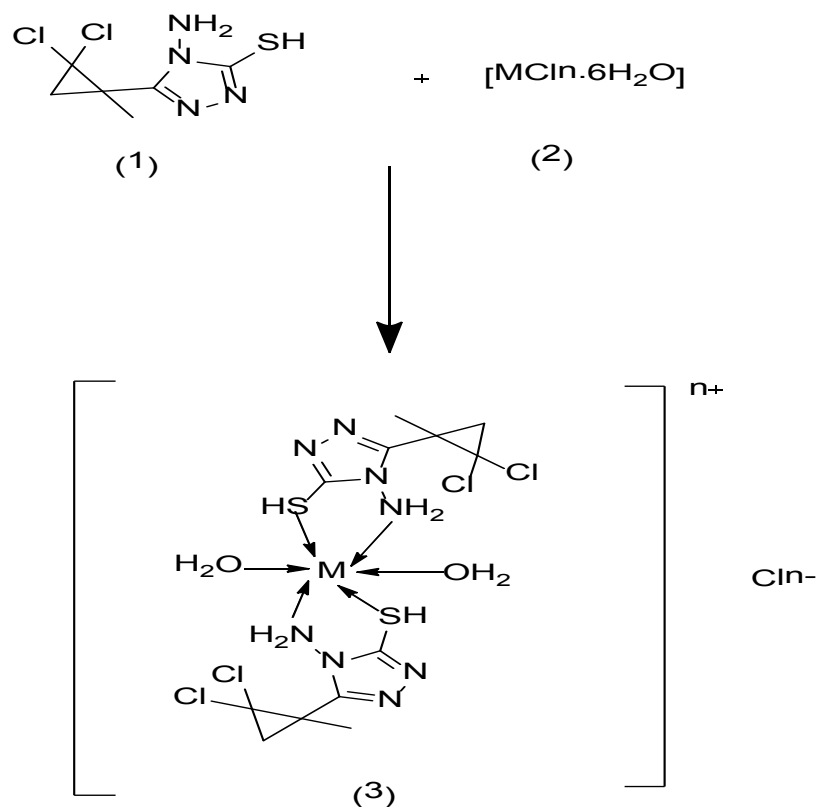

(1)

4-amino-5-(2,2-dichloro-1-methylcyclopropyl)-4*H*-1,2,4-triazole-3-thiol

Chemical Formula: $C_6H_8Cl_2N_4S$
Molecular Weight: 239.13

Fig. 1. Structural formula of ligand.

M=Cu (II), Cd (II) and Zn (II), n=2

Scheme 1. Preparation of Cu (II)-HL, Cd (II)-HL and Zn (II)- HL (HL=Traizole-Thiole) Chelates.

TABLE 1. Elemental and physical data of Traizole-Thiole ligand and its metal chelates.

Compound	Color (% yield)	M.P (°C)	% Found (Calcd.)					μeff (B.M)	Λm $\Omega^{-1}mol^{-1}cm^2$
			C	H	N	M	S		
HL (Traizole-Thiole)	Slight yellow (85)	120	30.11 (30.14)	3.12 (3.37)	22.98 (23.43)		.....	......	....
[CuHL$_2$.2H$_2$O]Cl$_2$ C$_{12}$H$_{20}$Cl$_6$CuN$_8$O$_2$S$_2$	Light green (80)	289	22.03 (22.22)	2.85 (3.11)	17.23 (17.27)	9.75 (9.89)	9.75 (9.80)	3.58	115
[CdHL$_2$.2H$_2$O]Cl$_2$ C$_{12}$H$_{20}$Cl$_6$CdN$_8$O$_2$S$_2$	White (87)	230	20.75 (20.66)	2.86 (2.81)	16.32 (16.06)	16.21 (16.11)	9.32 (9.19)	Diama	143
[ZnHL$_2$.2H$_2$O]Cl$_2$ C$_{12}$H$_{20}$Cl$_6$ZnN$_8$O$_2$S$_2$	White (85)	250	22.12 (22.15)	2.86 (3.10)	17.12 (17.22)	9.74 (9.86)	9.74 (10.05)	Diama	125

FT-IR spectra of Traizole-Thiole ligand and its metal chelates

The FT-IR of free ligand and the prepared chelates is shown in Fig. 2.

It shows dissimilarity between spectra of ligand and its chelates in order to identify the coordination sites involved in chelation process. The ligand spectra showed NH stretching band at 3297 cm^{-1}, NH$_2$ bands at 3200, 3240; bands at 2982 and CH group band a 2936 cm^{-1}. It also shows a band at 2750 cm^{-1} corresponds to SH group. The SH and NH$_2$ bands are reduced in intensity in the spectra of its metal chelates; which indicate

sharing of these groups in the complex formation process [46-48]. New bands are appeared in chart of chelates at 556–587 and 456–477 cm^{-1}. They are assigned as $\upsilon M–S$ and $\upsilon M–N$ stretching vibrations respectively. Consequently; the FT-IR confirms the tetra dentate behaviour of Traizole-Thiole ligand. The coordination sites of ligand are NNSS together with $2H_2O$ bind to the metal ion. The water molecules in the entity of metal chelates are confirmed by the appearance the broad bands at

3250- 3500 cm^{-1}. Therefore the proposed structures for these chelates are given in Fig. 3.

The proposed structures of Cu (II)-HL, Cd (II)-HL and Zn (II)-HL chelates (Fig. 3) are confirmed by mass, ^{1}H-NMR and XRD analyses.

Mass spectral studies (MS) of Traizole-Thiole chelates

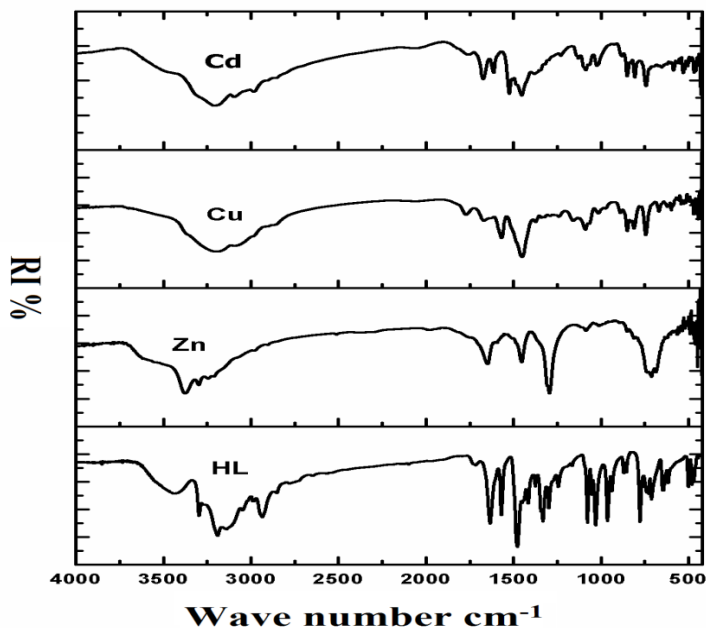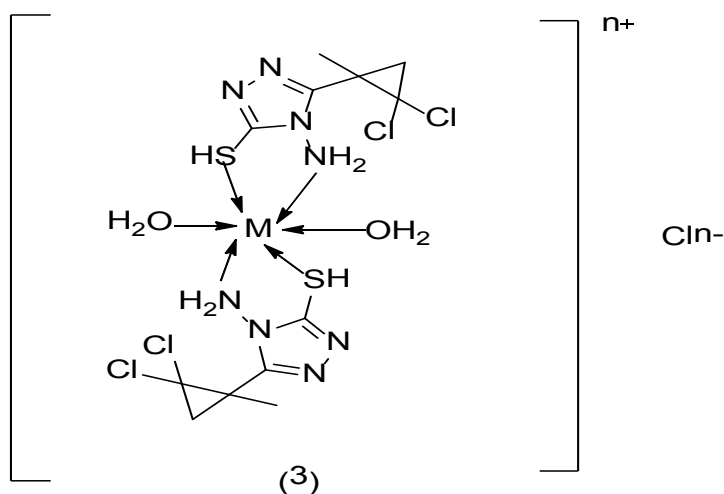The spectra of mass recorded of the ligand, Cu (II)-HL, Cd (II)-HL and Zn(II)-HL chelates

Fig. 2. FT-IR of HL, Cd-HL, Cu-HL chelates.

M=Cu (II), Cd (II) and Zn (II), n=2

Fig. 3. The proposed structures of Cu-HL, Cd-HL and Zn- HL chelates.

exhibited the molecular ion peaks at m/z 239, 648, 695 and 650 amu, which in coincidence with the proposed molecular weights 239, 648, 695 and 650 amu, for ligand and its metal chelates respectively. The molecular weights of the ligand and metal chelates were agreed with elemental and thermogravimetric analyses; which have been utilized to prove the suggested formula. These prove the stoichiometry of chelates as suggested in general formulae [M (HL)$_2$.2 H$_2$O] Cl$_2$.

^{1}H-NMR and ^{13}C-NMR of ligand and its metal chelates

The ^{1}H-NMR and ^{13}C-NMR of Traizole-Thiole and its metal chelates give the data**:** ^{1}H-NMR (500MHz, CDCl$_3$): δ = 1.62 (s, 3H, CH$_3$), 1.87 (d, 1H J = 8.6 Hz of CH); 2.16 (d, 1H, J = 7.6 Hz of CH), 5.60 (s, 2H, NH$_2$, exchanged with D$_2$O) and 13.69 (s, 1H, NH or SH are duterated with D$_2$O) ppm. The Traizole-Thiole and its metal chelates also give the data of ^{13}C NMR (125 MHz, CDCl$_3$): δ = 19.6 (CH$_3$), 28.3 (CH$_2$), 30.2 (CCH$_3$), 64.3(CCl$_2$), 152.4 (triazole C-5), 167.9 (triazole C-3) ppm. The bands of SH and NH$_2$ are disappeared after ligand coordination to metal cations (Cd(II) and Zn(II)); which may be attributed to the sharing of these groups in Zn-HL and Cd-HL chelates formation [49,50].

XRD Analyses

The XRD of the Cu (II)-HL, Cd(II)-HL and Zn (II)-HL chelates are given by Figs. (4-6).
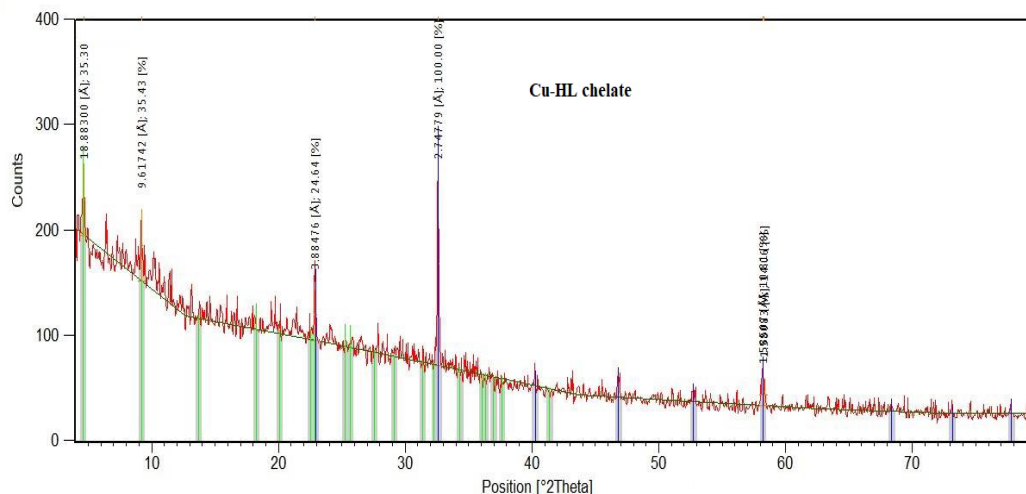
Fig. 4. Cu (II)-HL Chelate XRD.
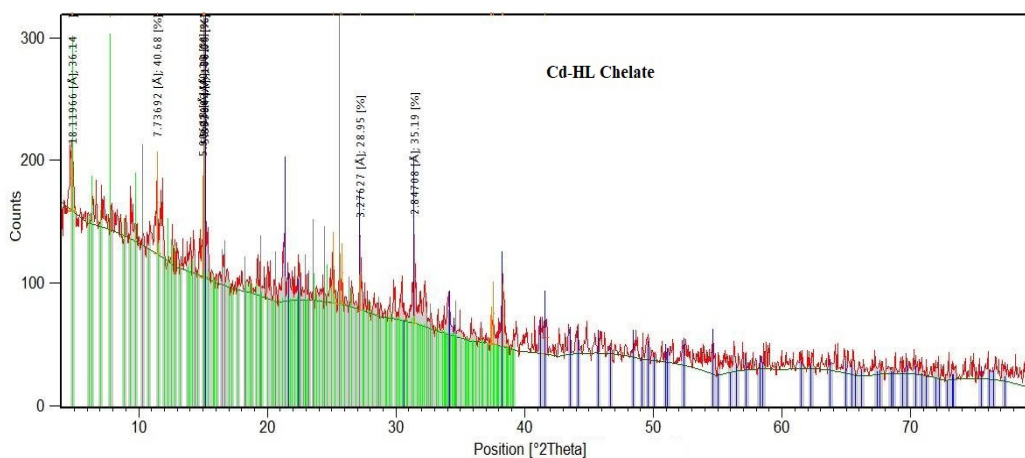
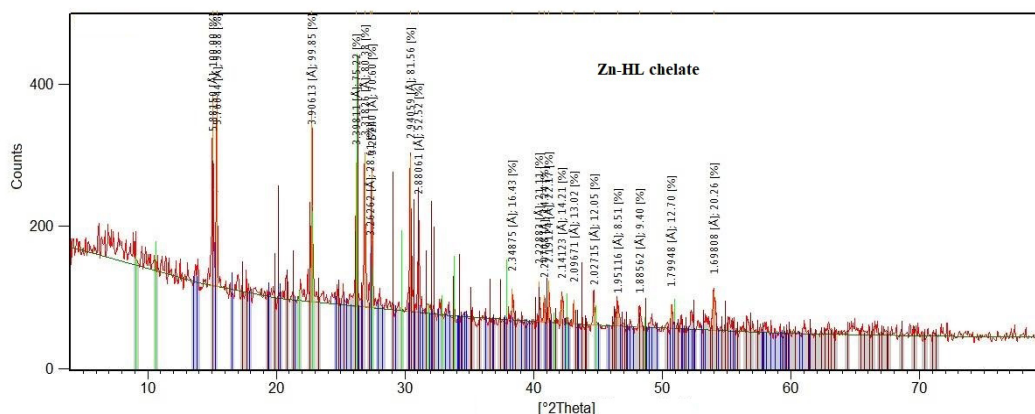

Fig. 5. Cd (II)-HL Chelate XRD.

Fig. 6. Zn (II)-HL Chelate XRD.

From these results and careful inspection of these curves it is concluded that; Cu (II)-HL Chelate (Fig. 4) is present in an amorphous form while both Cd (II)-HL and Zn (II)-HL Chelates (Figs. 5 and 6) are present in good crystalline structures with distinct lines of coordinated water molecules out of planes in proposed structural formulae of chelates given in Fig. 3.

Reflectance spectra and Magnetic susceptibility
The chelates diffused reflectance spectral data, bands positions and their transitions are important. All of these measurements are relies in the geometry of the given chelates. The diffused reflectance spectrum of the Cu (II)-HL chelate displayed the d–d transition band in the region14, 260 cm-1which is due to 2Eg → 2T2 g transition and also 25,231 and 32,543; which may be attributed to ligand to metal charge transfer. This d–d transition band strongly favours a distorted octahedral geometry around the metal ion. This geometry is further supported by its magnetic susceptibility value (2.1 BM) 28–30 [46-48, 51-54].

Electronic spectra of the Cd (II)-HL and Zn (II)-HL chelates exhibited a sharp band of high intensity at 22,332 and19, 765 cm^{-1}, respectively; which may have been due to the ligand–metal charge transfer.

Molar conductance of metal chelates
The measured molar conductance measurements in non-aqueous solutions had been used to study structures metal chelates depending upon the limits of their solubility. The measured values provide the degree of ionization of chelates. The higher the liberated molar ions from chelate entity will be the high its molar conductivity and vice versa. The molar conductance of the given chelates in DMF (10^{-3} M) solutions at 25 ± 2°C

are listed in Table 1. The molar conductance values of Cd (II)-HL, Zn (II)-HL and Cu (II)-HL chelates are found to be 143,125 and 115 Ω^{-1} mol^{-1} cm^2 respectively. These values refer to the 1:2 electrolytes and supported by the number of chloride ions detected in the proposed general formulae of these chelates [46-48, 51-54].

Thermal Analyses of Traizole-Thiole and its metal chelates
The thermal analyses of curves of Traizole-Thiole and its metal chelates are given in Fig. (7).

The thermogram of $[Cu(HL)_2(H_2O)_2].Cl_2$ chelate displays three stages of decomposition (Table 2).

The first stage at 25-200°C occures due to the loss of 2HCl molecules of mass loss = 11.64% (11.99%). The second stage, may be due to the loss of 2NH$_2$,H$_2$S and 2HCL molecule of mole mass = 21.86% (21.87%); it occures within the temperture range from 200 to 250°C. The third stage at 250-990 ^{o}C occures due to the loss of $C_{12}H_{10}Cl_2N_6OS$ molecules of mass loss = 54.34% (53.52%). leaving CuO as a residue.

The thermogram of $[Cd (HL)_2(H_2O)_2].Cl_2$ chelate displays the decomposition within three steps from 25 to 750 °C (Table 2). The first occurs at 25-180 °C is due to the loss of the 2HCl and 2H$_2$O molecules of mass loss of 15.23% (15.15%). The step two occurs at 180-320°C is due to the loss of 4HCl molecules with mass loss of 20.71% (20.40%). In the step number three, that occurs in temperature range 320-750°C; it may be attributed to the loss of the $C_{12}H_8N_8S_2$ molecule with mass loss of 47.42% (46.04%) leaving CdO as a residue for Cd(II)-HL chelate.
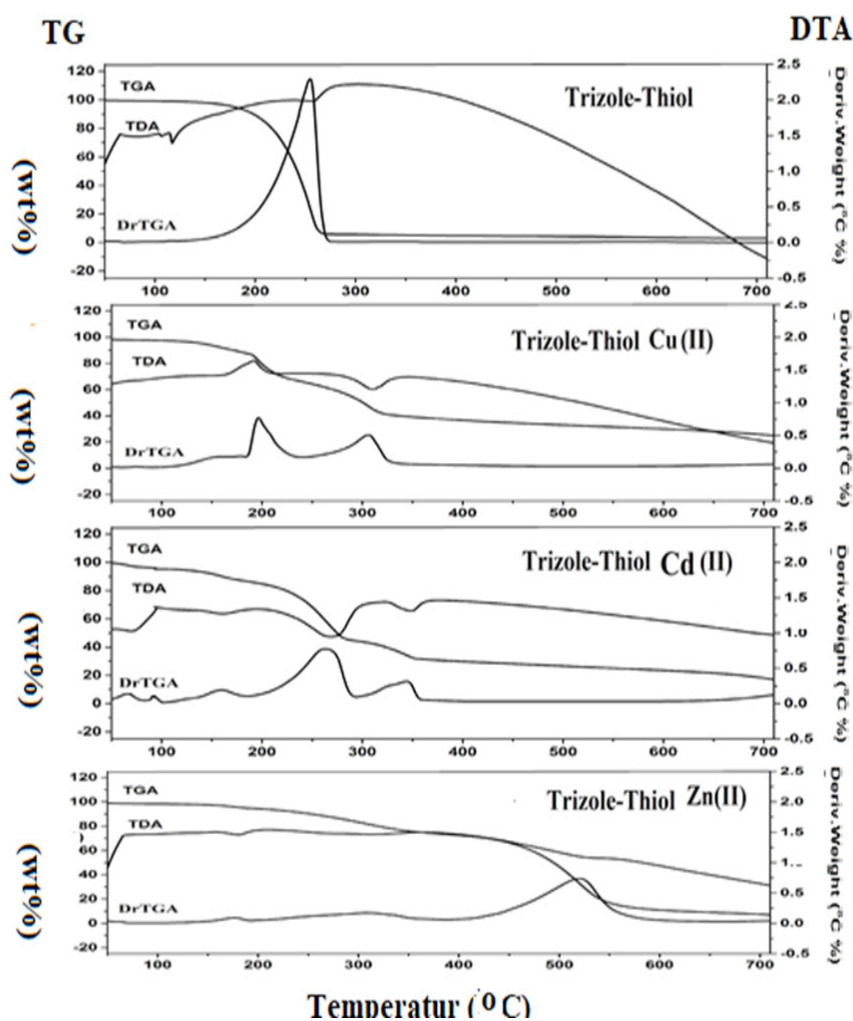
Fig .7. The thermal analyses of curves of Triazole-Thiole and its metal chelates.

TABLE 2. The thermal degradation results (TG and DTG) of both Traizole-Thiole ligand and its metal chelates

Compound	TG range (°C)	DTG_{max} (°C)	n*	Mass Loss Total mass Loss Calcd (Found) %	Assignment	Residue
HL (Triazole-Thiole)	50–180	100	1	6.30 (5.912)	Loss of CH_3	
	180–700	500	2	93.06 (93.69) 98.972 (99.99)	Loss of $C_5H_5Cl_2N_4S$	
[CuHL$_2$.2H$_2$O] Cl$_2$	25-200	150	1	11.64 (11.99)	-Loss of 2HCl	CuO 12.62
	200-250	220	1	21.86(21.87) 87.84 (87.38)	-Loss of $2NH_2,H_2S$ and 2HCL	
	250-990	700	1	54.34(53.52)	-Lossof $C_{12}H_{10}Cl_2N_6OS$	
[CdHL$_2$.2H$_2$O] Cl$_2$	25-180	100	1	15.23 (15.15)	-Loss of 2HCl and $2H_2O$.	CdO 18.41
	180-320	250	2	20.71 (20.40) 83.36 (81.59)	-Loss of 4HCl	
	320-750	550	2	47.42 (46.04)	-Loss of $C_{12}H8N_8S_2$	
[ZnHL$_2$.2H$_2$O] Cl$_2$	25-200			5.26 (5.339)	-Loss of NH_2.	ZnO 12.6
	200-400	183	1	24.77 (23.26) 88.^6 (87.4)	-Loss of 4HCl andH_2O.	
		300	1			
	400-800	628	1	58.83(58.801)	-Loss of $C_{12}H_{12}Cl_2N_7S_2$	

The thermogram of $[Zn(HL)_2(H_2O)_2].Cl_2$ chelates displays the decomposition in three steps at temperature 25-800 °C (Table 2). The stage number one occurs at 25-200°C due to the loss of NH_2 molecule with the estimated mass loss of 5.26% (5.339%). The second stage, occurs at 200-400 °C is due to the loss of 4HCl and H_2O molecules of 24.77% (23.26%). The third step occurs at temperature range 400-800 °C as a result of the loss of $C_{12}H_{12}Cl_2N_7S_2$ molecule of 58.83% (58.801%) leaving ZnO as a residue.

The thermodynamic calculations coming from these thermal data are given in Table 3.

These data refer to the high thermal stability of the given chelates; which may be attributed to chelate ring structures of these chelates represented in Fig. 3. This stability increases in the following order as Cd (II)-HL (E^*kJmol^{-1} = 540.33 to 218.24) > Cu (II)-HL (E^*kJmol^{-1} = 78.10 to 422.49) > Zn (II)-HL (E^*kJmol^{-1} = 91.78 to 235.29) > HL (E^*kJmol^{-1} = 37.86 to 30.31) depending upon the values of the calculated activation energy at different temperature ranges. This ordering is confirmed by enthalpy of activation ΔH^* $kJmol^{-1}$ as Cd (II)-HL (533.96 to 211.84) > Cu (II)-HL (71.69 to 358.49) > Zn (II)-HL (277.75 to 346.73) > HL (31.46 to 29.76) There is another ordering depending upon the start and on set temperature range of decomposition Cu (II)-HL (Decomp. Temp.°C =25 to 990) > Zn (II)-HL (Decomp. Temp.°C = 25 to 800) > Cd (II)-HL (Decomp. Temp.°C = 25 to 750) > HL (Decomp. Temp.°C = 50 to 700).

Theoretical Molecular Orbital Calculations (TMOCs)

The elemental analyses proved that, two ligand molecules are coordinated with Cu (II), Cd(II) and Zn (II) forming $[M(HL)_2.2H_2O]Cl_2$ chelates. TMOCs are used to prove the nature and stability of these chelates. The calculated geometrical parameters are bond angles, bond lengths and dihedral angles, natural charges on active centers and energetic of the optimized ground state for the studied chelates. These geometrical parameters together with the practical spectroscopic data proved that the metal ions are coordinated to the ligand via (N, O and S) atoms forming stable chelates.

The optimized geometrical parameters (bond lengths, bond angles and dihedral angles), natural charges on active centers and energetic of the ground state for the studied chelates were computed and analyzed. From the elemental analyses and spectroscopic data, metal ions coordinated to the ligand via N, O and S atoms forming these chelates. The ligand HL actually coordinatedvia N, O and S atoms to Cu (II), Zn (II) and Cd (II) forming chelates of the general formula $[M(HL)_2(H_2O)_2]$.

Geometry of the chelates

In this research; vector of the dipole moment, energetic, dipole moment, bond lengths, bond angles and dihedral angles of were calculated using numbering system of optimized geometry of novel ligand and its studied metal chelates.

Figure 8 presents the optimized geometry, numbering system, and vector of the dipole moment, energetic, dipole moment, bond lengths, bond angles and dihedral angles of all metal chelates studied in this work.

The optimized geometrical calculated data are given Tables 4-8.

TABLE 3. The calculated thermodynamic parameters from TG and TG data of the thermal decomposition of both Traizole-Thiole and its metal chelates.

| Complex	Decomp. Temp. °C	A s⁻¹	E^* kJmol⁻¹	ΔS^* JK⁻¹mol⁻¹	ΔH^* kJmol⁻¹	ΔG^* kJmol⁻¹
HL (Triazole-Thiole)	50–180	$1.20\ 10^7$	37.86	-167.56	31.46	185.70
	180–700	$1.55\ 10^6$	30.31	-55.50	29.67	130.24
[Cu(HL)₂.2H₂O]Cl₂	25-200	8.56×10^8	78.10	-167.10	71.69	568.56
	200-250	8.56×10^6	196.20	-301.13	189.80	418.58
	250-990	4.19×10^5	422.49	-145.19	358.49	147.54
[Cd(HL)₂.2H₂O]Cl₂	25-180	1.13×10^7	540.33	-105.01	533.96	273.96
	180-320	1.90×10^6	218.24	-231.18	211.84	339.95
	320-750	3.64×10^4	380.91	-504.63	374.51	136.98
[Zn(HL)₂.2H₂O]Cl₂	25-200	3.99×10^6	91.78	-145.60	277.75	114.78
	200-400	7.55×10^8	353.23	-357.53	346.73	716.86
	400-800	2.46×10^7	235.29	-252.48	228.89	346.59
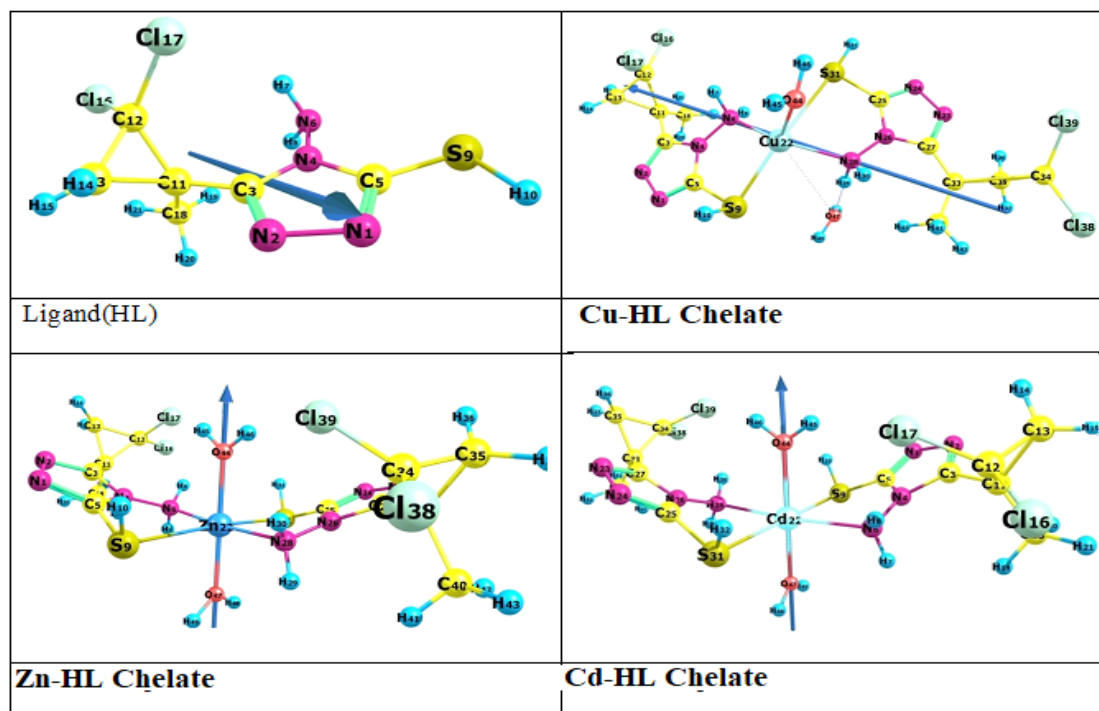
Fig. 8. The optimized geometry, numbering system, vector of dipole moment of HL, Cu(II)-HL, Zn(II)-HL and Cd(II)-HL chelates using B3LYP/GENECP level of calculation.

Tables 4 represents selected bond length (A°), bond angles and dihedral angles, (degree) of Cu(II)-HL, Zn(II)-HL and Cd(II)-HL chelates and Table 5 represents natural charge on coordinated atoms of HL and the same chelates.

From the data in Tables 4 and 5; it is clear that in Cu(II)-HL, Zn(II)-HL and Cd(II)-HL chelate, the metal ion coordinates with N6 and S9 from the ligand with the sequences N6N4C5S9 and N24N22C21S31 to form a five-member ring and with O44, O47 from two water molecule, Therefore, the form of slightly distorted regular octahedral geometry is expected for all the studied chelates. Most M-N, M-S and M-O bonds show elongation upon complexation between 2.1 to 2.7 A⁰. The length of the coordinate covalent bonds between metal and ligand site, i.e. M-N, M-S and M-O, are too long compared to the typical MX bond lengths [26]. The too long M-O, M-S and M-N bonds in the studied chelates mean that the ionic character of these bonds is small. The calculated values of bond angles between metal ion and binding sites (Tables 1) N4N6M, C5S9M, N6MS31, S9MN28 and S31MO44 vary between 81 and 110 which compare nicely with the experimental data as obtained from X-ray analysis for OH in the moiety of chelates [27]; which indicate a distorted octahedral

geometry as expected for all the studied chelates. The dihedral angles around metal ion, i.e. C3N4N6M, C5N4N6M, N1C5S9M, N4N6MS9, S9MN28N26 and N4N6MS31, are close from 0 or 180° which indicate that the metal ion is in the same molecular plane of the ligand and other coordination with water N4N6MO44, N4N6MO47 and O44MN28N26 are close to 90°.

Natural charges and natural population

The natural population analysis performed on the electronic structures of the studied chelates clearly describes the distribution of electrons in various sub-shells of their atomic orbits. The natural charges on the coordinating sites in the core, valence and Rydberg sub-shells and natural electronic configuration of the metal in the studied chelates are presented in Table 6.

The most electronegative centers are accumulated on N6, S9, N28, S31, O44 and O47. These electronegative atoms have a tendency to donate electrons. Whereas, the most electropositive atoms are Cu, Zn and Cd have a tendency to accept electrons. The central metal ion in the Cu, Zn and Cd chelates received 1.74e, 0.93e, and 0.86e from the donating sites of the ligands with electronic configuration $3d^{4.96}$, $3d^{9.99}$, $3d^{9.99}$ from the active sites of the ligands respectively.

TABLE 4. The selected bond length (Aᵒ), bond angles and dihedral angles, (degree) of Cu(II), Zn(II) and Cd(II) complexes B3LYP/ genecp level of theory.

	Cu(II)	Zn(II)	Cd(II)
R(N6,M)	2.153	2.226	1.468
R(S9,M)	2.429	2.582	2.717
R(N28,M)	2.240	2.226	2.469
R(M,S31)	3.179	2.582	2.717
R(M,O44)	2.191	2.200	2.432
R(M,O47)	4.000	2.256	2.444
R(N1,C5)	1.299	1.295	1.296
R(C3,N4)	1.384	1.391	1.392
R(N4,C5)	1.379	1.379	1.380
R(N4,N6)	1.411	1.412	1.411
R(C5,S9)	1.774	1.774	1.777
R(N6,H7)	1.026	1.022	1.021
R(S9,H10)	1.354	1.354	1.354
R(N24,C25)	1.340	1.295	1.296
R(C25,N26)	1.357	1.379	1.380
R(C25,S31)	1.737	1.774	1.777
R(N26,C27)	1.413	1.391	1.392
R(N26,N28)	1.416	1.412	1.411
R(N28,H29)	1.031	1.022	1.021
R(S31,H32)	1.354	1.354	1.354
R(O44,H45)	0.966	0.969	0.968
R(O47,H48)	0.966	0.968	0.967
A(C3,N4,C5)	104.51	104.38	104.15
A(C3,N4,N6)	129.33	129.37	128.70
A(C5,N4,N6)	125.69	125.41	125.97
A(N1,C5,N4)	110.50	110.76	110.87
A(N1,C5,S9)	126.16	126.75	125.50
A(N4,C5,S9)	123.33	122.47	123.56
A(N4,N6,H7)	107.00	109.25	109.49
A(C5,S9,H10)	96.99	96.46	95.76
A(C5,S9,M)	92.78	91.62	92.60
A(H10,S9,M)	105.62	101.10	101.63
A(S9,M,O44)	117.39	92.82	90.24
A(S9,M,O47)	71.33	87.20	89.78
A(S31,M,O44)	83.18	92.80	90.21
A(S31,M,O47)	93.11	87.18	89.77
A(N24,N23,C27)	109.96	109.04	108.97
A(N24,C25,S31)	123.82	126.75	125.51
A(N26,C25,S31)	125.79	122.47	123.56
A(C25,N26,C27)	104.87	104.38	104.15
A(C25,N26,N28)	124.36	125.41	125.97
A(C27,N26,N28)	130.70	129.37	128.71
A(M,S31,C25)	90.83	91.61	92.59
A(M,S31,H32)	174.02	101.08	101.64
A(C25,S31,H32)	92.48	96.46	95.76
A(M,O44,H45)	123.25	126.34	126.61
A(M,O47,H48)	128.18	126.88	127.02
D(N6,N4,C5,N1)	174.45	171.78	169.92
D(N6,N4,C5,S9)	-6.04	-9.66	-12.77
D(N1,C5,S9,M)	172.78	-158.68	-152.56
D(N4,C5,S9,H10)	111.79	124.37	132.50
D(N4,C5,S9,M)	5.67	23.01	30.53
D(C5,S9,M,O44)	115.59	66.47	61.55
D(C5,S9,M,O47)	-110.45	-113.54	-118.47
D(H10,S9,M,O44)	17.53	-30.44	-34.88
D(H10,S9,M,O47)	-151.64	149.55	145.10
D(C5,S9,S31,C25)	-151.65	133.08	123.05
D(C5,S9,S31,H32)	-30.22	35.77	26.60
D(N6,M,S31,C25)	-149.39	154.49	-25.43
D(N6,M,S31,H32)	86.98	57.59	-121.86
D(N6,M,N28,N26)	-66.03	-71.71	-65.24
D(N6,M,N28,H29)	-61.73	165.44	171.04

TABLE 5. Natural charge on coordinated atoms of HL, Cu (II), Zn (II) and Cd (II) chelates using B3LYP/GENECP level of theory.

Atom	HL	Cu(II)	Zn(II)	Cd(II)
N6	-0.616	-0.322	-0.675	-0.661
N28		-0.326	-0.675	-0.661
S9	0.076	0.050	0.129	0.122
S31		0.079	0.129	0.123
O44		-0.464	-0.958	-0.963
O47		-0.481	-0.950	-0.956

TABLE 6. Natural charge, natural population and natural electronic configuration of metal ions in the studied complexes using B3LYP/ GENECP level of theory.

Complex	Atomic No.	Natural charge	Natural population				Natural configuration
			Core	Valence	Rydberg	Total	
Cu(II)	29	0.2575	8.99956	5.2367	0.00623	14.2425	$[core]4S^{0.14}3d^{4.96}4p^{0.14}$
Zn(II)	30	1.07277	17.99939	10.89888	0.02895	28.92723	$[core]4S^{0.45}3d^{9.99}4p^{0.46}4d^{0.01}$
Cd(II)	48	1.14103	35.99929	10.84238	0.0173	46.85897	$[core]4S^{0.48}3d^{9.99}4p^{0.37}4d^{0.01}$

Global Reactivity Descriptors (GRD)

The calculated data of the global reactivity descriptor using B3LYP/GENECP level of theory; are given in Tables (7 and 8) and the graphical representation of these data is given in Figs. (9 and 10).

They include HOMO, LUMO, energy gap (Eg), chemical hardness (h), electronegativity (X), chemical potential (V), electron affinity (A), ionization potential (I) and chemical softness(S). The frontier molecular orbital (FMO) energies of the studied complexes were calculated using B3LYP/GENECP and presented in Figs. (9, 10). HOMO energy characterizes the electron donating ability, while LUMO energy characterizes the electron withdrawing ability. Energy gap (Eg) between HOMO and LUMO characterizes the molecular chemical stability which is a critical parameter in determining molecular electrical transport properties because it is a measure of electron conductivity. The results in (Figs. 9 and 10) and Table 7 indicate that the smaller the energy gap the easier the charge transfer and the polarization occurs within the molecule. Furthermore, the order of increasing reactivity is:

Cu-HL > Cd-HL > Zn-HL >> HL. Using HOMO and LUMO energies, ionization potential and electron affinity can be expressed as $I \sim -E_{HOMO}$, $A \sim - E_{LUMO}$ as shown in Table 7. The variation of electronegativity (X) values is supported by electrostatic potential, for any two molecules, where electron will be partially transferred from one of low X to that of high X. The results show that the order of decreasing X (increasing CT within the molecules) is: Cu-HL > Cd-HL > Zn-HL >> HL.

The chemical hardness (η) = (I-A)/2, electronegativity (X) = (I +A)/2, chemical potential (V) = - (I+E)/2 and chemical softness(S) = 1/2η values are calculated and presented in Table 8.

The results of small η values for the studied compounds reflect the ability of charge transfer inside the molecule. Therefore, the order of increasing the charge transfer within the molecule is: Cu-HL > Cd-HL > Zn-HL >> HL. Considering η values, the higher the η values, the harder is the molecule and vice versa.

TABLE 7. Global reactivity descriptors of HL, Cu (II), Cd(II) and Zn (II) chelates using B3LYP/GENECP level of theory.

Parameters	HL	Cu(II)	Zn(II)	Cd(II)
ET,au	-1771.15624	-5335.27800	-5474.17211	-3862.53651
EHOMO,au	-0.24279	-0.44772	-0.48544	-0.48038
ELUMO,au	-0.03675	-0.37135	-0.29466	-0.32145
Eg,eV	5.606	2.078	5.191	4.325
μ, D	1.441	5.789	3.759	3.992
I,eV	6.606	12.183	13.209	13.071
A,eV	1.000	10.105	8.018	8.747
X,eV	3.803	11.144	10.614	10.909
η,eV	2.803	1.039	2.596	2.162
S,eV	0.178	0.481	0.193	0.231
V,eV	-3.803	-11.144	-10.614	-10.909
ω	2.212	1.956	0.823	0.988
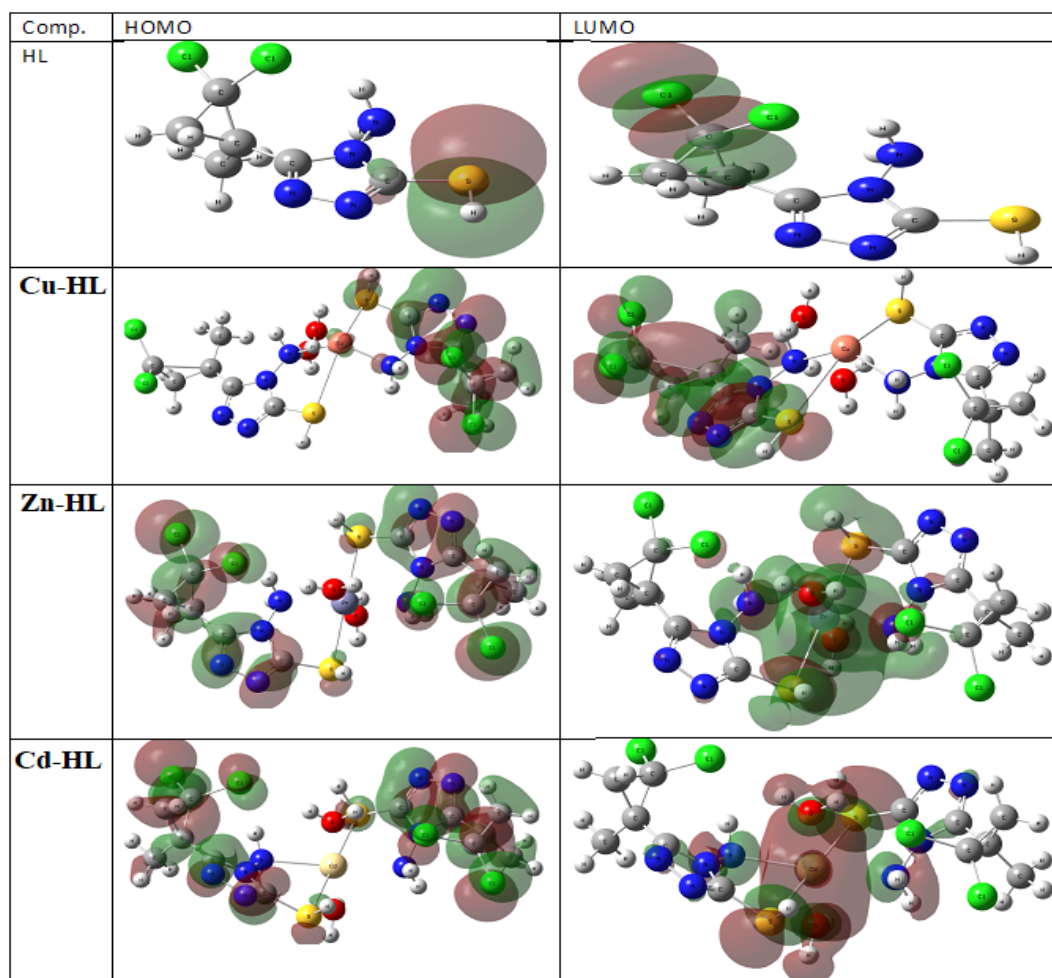
Fig. 9. HOMO-LUMO charge density maps of HL, Cu-HL, Zn-HL and Cd-HL chelates using B3LYP/GENECP level of calculation.
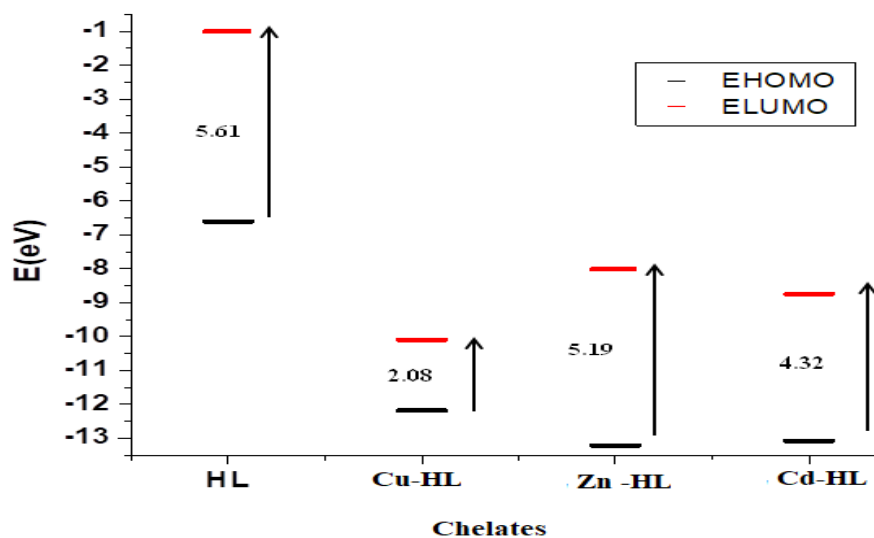
Fig. 10. Relation between EHOMO, ELUMO and E$_{gap}$ of HL, Cu-HL, Zn-HL and Cd-HL chelates using B3LYP/ GENECP level of theory.

TABLE 8. Total static dipole moment (μ), The mean polarizability (< α >), The anisotropy of the polarizability (< Δα >) and the mean first-order hyper-polarizability (β (esu)) for Cu(II), Zn(II), Cd(II) and HL complexes using B3LYP/GENECP level of theory.

	Urea	Cu-HL	Zn-HL	Cd-HL	HL
x,D		5.764	0.022	0.042	-0.698
y,D		-0.537	-0.158	-0.661	-1.149
z,D		0.036	-3.756	-3.937	0.519
μ,D	1.320	5.789	3.759	3.992	1.441
αxx,au		554.138	377.322	388.830	180.264
αxy,au		-49.799	-22.360	-19.509	3.665
αyy,au		330.828	306.170	311.953	128.629
αxz,au		55.086	1.648	4.708	-9.531
αyz,au		2.807	-2.699	-10.217	5.259
αzz,au		252.006	244.692	254.280	120.196
<α>,esu		5.6163E-23	4.5849E-23	4.7177E-23	2.1196E-23
<Δα>,esu		4.0225E-23	1.7036E-23	1.7326E-23	8.3472E-24
βxxx		2819.493	3.978	12.566	-240.471
βxxy		-927.487	-9.911	-65.086	-71.691
βxyy		564.123	1.058	-14.459	16.125
βyyy		51.070	-8.669	-50.054	-8.038
βxxz		-79.604	-235.550	-393.183	45.021
βxyz		50.425	8.196	-45.211	-12.734
βyyz		-13.561	-69.031	-97.403	17.998
βxzz		18.235	-2.408	9.094	8.605
βyzz		5.573	-0.259	3.323	-24.563
βzzz		135.843	-146.124	-176.337	-17.178
<β>,esu	1.95E-31	3.0339E-29	3.8972E-30	5.8424E-30	2.1077E-30

Non-linear optical properties (NLO):

No experimental or theoretical investigations were found addressing NLO for the studied novel chelates; therefore, this triggered our interest to undertake this study. NLO properties is the key functions of frequency shifting, optical modulation, switching, laser, fiber, optical materials logic and optical memory for the emerging technologies in areas such as telecommunications, signal processing and optical inter connections [46-48, 51-54]. In order to investigate the relationship between molecular structure and NLO, the polarizibilities and hyperpolarizibilities of the studied chelates are calculated using B3LYP/GenECP level of theory (Table 8). Total static dipole moment (μ), the mean polarizability$<\alpha>$, the anisotropy of the polarizability ($< \Delta\alpha >$) and the mean first-order hyperpolarizibility (β) of the studied complexes are listed in Table 8. The polarizibilities and first-order hyperpolarizibilities are reported in atomic units (a.u.), the calculated values have been converted into electrostatic units (esu) using conversion factor of 0.1482 x 10^{-24} esu for α and 8.6393 x 10^{-33}esu for β. Urea is a standard prototype used in NLO studies. In this study, Urea is chosen as a reference as there were no experimental values of NLO properties of the studied chelates. The magnitude of the molecular hyperpolarizibility β is one of the key factors in NLO system. The analysis of the β parameter show that Cu (II)-HL chelate is ~3.7 times higher than (UREA), while Zn (II)-HL, Cd (II)-HL chelates and HL are 0.51, 0.81, 0.46 to the reference respectively. Therefore, the Cu-HL chelate is very an efficacious candidate for NLO materials rather than other studied chelates.

Biological activity

The studied ligand is considered one of an important class of compounds in medical and pharmaceutical fields. They can be used in biological applications as antibacterial and antifungal reagents. The results of antimicrobial activities of the prepared triazole ligand and its metal chelates are presented in Table 9.

These results are obtained by applying diffusion agar method [55-57]. The antibacterial and antifungal activities were tested using Streptomycin as a reference. The tested organisms are Gram-positive (*Staphylococcus aureus* ATTC 12600), Gram-negative (*Escherichia coli* ATTC 11775 and) bacteria, two fungus (*Aspergillus flavus* and *Candida albicans*). The antibacterial and antifungal activity was evaluated by measuring the inhibition zone (mm). The data obtained are graphically represented and in Fig. (11).

TABLE 9. Biological activity of HL ligand and its Cu-HL, Cd-HL and Zn-HL chelates.

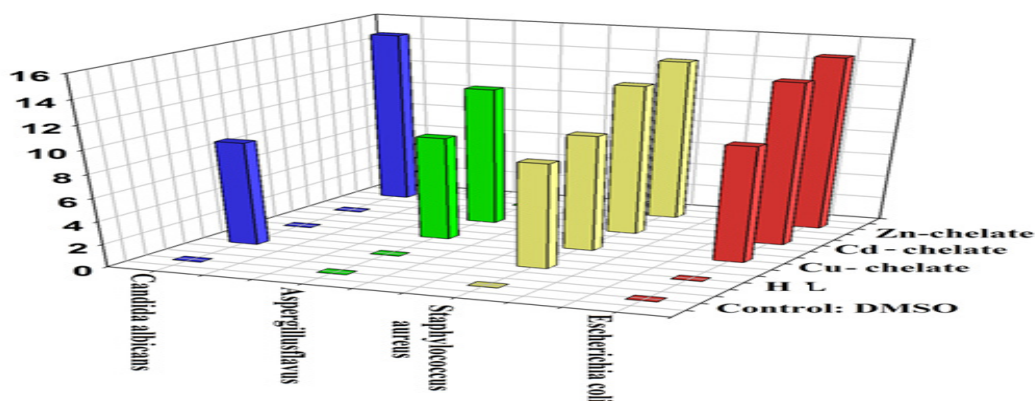| Sample	Inhibation zone diameter (mm/mg sample)			
	Escherichia coli (G⁻)	Staphylococcus aureus G⁺	Aspergillusflavus (Fungus)	Candida albicans (Fungus)
Control: DMSO	0.0	0.0	0.0	0.0
HL	0.0	9	0.0	9
Cu -HL	10	10	9	0.0
Cd -HL	14	13	12	0.0
Zn-HL	15	14	0.0	15
Amoxicillin	13	12	9	14

Fig. 11. Graphical representation of biological activity of HL ligand and its Cu -HL, Cd-HL and Zn-HL chelates.

These data refer to Zn-HL chelate is the best antimicrobial agent for all microbial organism. On the other hand, it is found that the Cd-HL chelate is more active than Cu-HL than HL toward the Gram-positive (*Staphylococcus aureus* ATTC 12600), Gram-negative (*Escherichia coli* ATTC 11775 and) bacteria and (*Aspergillus flavus*) fungi. Comparing these results with theoretical calculation of electronegativity values (X) it detected that; it is the reverse order of decreasing X (increasing CT within the molecules) Cu-HL > Cd-HL > Zn-HL >> HL. This is may be attributed to the variation of the electron cloud within the entity of chelate as confirmed by HOMO and LUMO calculations (Figs. 8 and 9) and in Table 7. These results refer to concentration of electron cloud around biologically active sulphur centre of HL in moiety of Zn-HL chelate > Cd-HL>Cu-HL> free HL ligand; which is in good correlation with their tested antimicrobial activities. Also this trend is correlated to theoretical calculations of energy gap values (eV) in Fig. 10, (Zn- HL = 5.19, Cd-HL = 4.32 and Cu-HL = 2.08) and in reverse order to electronegativity (X) values. The variation of electronegativity (X) values is supported by electrostatic potential, for any two molecules, where electron will be partially transferred from one of low X to that of high X. The results show that the order of decreasing X (increasing CT within the molecules) is: Cu-HL > Cd-HL > Zn-HL >> HL.

Conclusions

Structural and molecular properties of Triazole-Thiole (HL) toward the transition metal ions namely Cu (II), Cd (II) and Zn (II) have been studied by elemental analyses, magnetic measurements, electronic, FT-IR, ^{1}H-NMR and thermal analyses (TGA and DTA). All computations were carried out using Gaussian 09W software package. The theoretical and practical spectra of both ligand and its metal chelates were correlated and found to be confirming each other. The ligand and its metal chelates had been examined against Gram-positive (*Staphylococcus aureus* ATTC 12600), Gram-negative (*Escherichia coli* ATTC 11775 and) bacteria, two fungus (*Aspergillus flavus* and *Candida albicans*) to give the order of the best antimicrobial activity Zn-HL> Cd-HL> Cu-HL >> HL as a general trend in relation to transition metal cation standard Amoxicillin. Also this trend is correlated to theoretical calculations of energy gap values in eV (Zn- HL = 5.19, Cd-HL = 4.32 and Cu-HL = 2.08) and in reverse order

to electronegativity (X) values. The variation of electronegativity (X) values is supported by electrostatic potential, for any two molecules, where electron will be partially transferred from one of low X to that of high X. The results show that the order of decreasing X (increasing CT within the molecules) is: Cu-HL > Cd-HL > Zn-HL >> HL.

Acknowledgement

References

1. Zayed E. M., Hindy A. M., Mohamed G. G., coordination behaviour, molecular docking, density functional theory calculations and biological activity studies of some transition metal complexes of bis☐Schiff base ligand, *Appl. Organomet. Chem.,* e4525 (2018).

2. Gökce H., Öztürk N., Ceylan Ü., Alpaslan Y. B., Alpaslan G., Thiol–thione tautomeric analysis, spectroscopic (FT-IR, Laser-Raman, NMR and UV–vis) properties and DFT computations of 5-(3-pyridyl)-4H-1, 2, 4-triazole-3-thiol molecule *Spectrochim. Acta. Part. A*, **163**, 170-180 (2016),.

3. Aziz A. A. A., Elantabli F. M., Moustafa H., El-Medani S. M., Spectroscopic, DNA binding ability, biological activity, DFT calculations and non linear optical properties (NLO) of novel Co(II), Cu(II), Zn(II), Cd(II) and Hg(II) complexes with ONS Schiff base, *J. Mol. Struct.* **1141**, 563-573 (2017).

4. Tyagi P., Tyagi M., Agrawal S., Chandra S., Ojha H., Pathak M., Synthesis, characterization of 1,2,4-triazole Schiff base derived 3d-metal complexes: Induces cytotoxicity in HepG2, MCF-7 cell line, BSA binding fluorescence and DFT study. *Spectrochim. Acta. Part. A.,* **171**, 246 (2017).

5. Olar R., Calu L., Badea M., Chifiriuc M. C., Bleotu C., Velescu B., Stoica O., Ionita G., Stanica N., Silvestro L., Thermal behaviour of some biologically active species based on complexes with a triazolopyrimidine pharmacophore, *J. Therm. Anal. Calorim.,* **127**, 685 (2017).

6. DİLBER G., DURMUŞ M., Kantekin H., Investigation of the photophysical and photochemical behavior of substituted zinc

phthalocyanines and their water-soluble quaternized derivatives, *Turkish Journal of Chemistry,* **41**, 917 (2017).

7. Fizer M., Sukharev S., Slivka M., Mariychuk R., Lendel V., Preparation of bisthiourea and 5-Amino-4-benzoyl-1,2,4-triazol-3-thione complexes of Copper (II), Nickel and Zinc and their biological evolution, *J. Organomet. Chem.,* 804 (2016).

8. Zayed E. M., Ismail E. H., Mohamed G. G., Khalil M. M., Kamel A. B., Synthesis, spectroscopic and structural characterization, and antimicrobial studies of metal complexes of a new hexadentate Schiff base ligand. Spectrophotometric determination of Fe(III) in water samples using a recovery test, *Monatsh. Chem.,***145**, 755 (2014).

9. Badea M., Calu L., Chifiriuc M. C., Bleotu C., Marin A., Ion S., Ioniţă G., Stanică N., Măruţescu L., Lazăr V., Thermal behaviour of some novel antimicrobials based on complexes with a Schiff base bearing 1,2,4-triazole pharmacophore, *J. Therm. Anal. Calorim.,* **118**,1145 (2014).

10. Khanmohammadi H., Erfantalab M., Azimi G., New acyclic 1, 2, 4-triazole-based Schiff base hydrazone: Synthesis, characterization, spectrophotometric and computational studies, *Spectrochim Acta Part A.,***105**, 338 (2013).

11. Calu L., Badea M., Falcescu D., Duca D., Marinescu D., Olar R., Thermal study on complexes with Schiff base derived from 1, 2, 4-triazole as potential antimicrobial agents, *J. Therm. Anal. Calorim.,* **111**, 1725 (2013).

12. Avcı D., Atalay Y., Şekerci M., Dinçer M., Molecular structure and vibrational and chemical shift assignments of 3-(2-Hydroxyphenyl)-4-phenyl-1*H*-1,2,4-triazole-5-(4*H*)-thione by DFT and *ab initio* HF calculations, *Spectrochim. Acta. Part.,* **73**, 212 (2009).

13. Zayed E. M., Zayed M. A., Abd El Salam H. A., Nawwar G. A., Synthesis, structural characterization, density functional theory (B3LYP) calculations, thermal behaviour, docking and antimicrobial activity of 4-amino-5-(heptadec-8-en-1-yl)-4H-1,2,4-triazole-3-thiol and its metal chelates. *Appl. Organomet. Chem.,* e4535 (2018).

14. Hassan W. M., Zayed E. M., Elkholy A. K., Moustafa H., Mohamed G. G.. Spectrochim. Spectroscopic and density functional theory investigation of novel Schiff base complexes, *Acta. Part.,* **103**, 378 (2013).

15. Ghassemzadeh M., Firouzi R., Shirkhani S., Amiri S., Neumueller B., New dinuclear copper(I) metallacycles containing *bis*-Schiff base ligands fused with two 1,2,4-triazole rings: Synthesis, characterization, molecular structures and theoretical calculations, *Polyhedron*, **69**, 188 (2014).

16. Badea M., Pătraşcu F., Korošec R. C., Bukovec P., Raita M., Chifiriuc M. C., Măruţescu L., Bleotu C., Velescu B., Marinescu D., Thermal, spectral, magnetic and biologic characterization of new Ni(II), Cu(II) and Zn(II) complexes with a hexaazamacrocyclic ligand bearing ketopyridine moieties, *J. Therm. Anal. Calorim.,* **118**, 1183 (2014).

17. El Metwally N. M., Arafa R., El-Ayaan U., Molecular modeling, spectral, and biological studies of 4-formylpyridine-[4] N-(2-pyridyl) thiosemicarbazone (HFPTS) and its Mn(II), Fe(III), Co(II), Ni(II), Cu(II), Cd(II), Hg(II), and UO_2(II) complexes, *J. Therm. Anal. Calorim.,* **115**, 2357 (2014).

18. Zayed E., Zayed M. A., Noamaan M.A., Abd El Salam H.A., Novel Triazole Thiole ligand and some of its metal chelates: Synthesis, structure charactertization, thermal behavior in comparison withcomputational caculations andbiological activities. *Computational Biology and Chemistry* **78**, 260–272 (2019).

19. Bharty M., Dani R., Nath P., Bharti A., Singh N., Prakash O., Singh R. K., Butcher R.., Syntheses, structural and thermal studies on Zn(II) complexes of 5-aryl-1,3,4-oxadiazole-2-thione and dithiocarbamates: Antibacterial activity and DFT calculations, *Polyhedron*., **98**, 84 (2015).

20. Frisch M., Trucks G., Schlegel H., Scuseria G., Robb M., Cheeseman J., Scalmani G., Barone V., Mennucci B., Petersson G.. Inc., Wallingford, CT.; 6492 (2010).

21. Becke A. D., Density-functional exchange-energy approximation with correct asymptotic behavior, *Phys. Rev. A,* **38**, 3098 (1988).

22. Becke A. D., Densityfunctional thermochemistry. III. The role of exact exchange. *J. Chem. Phys.,* **98**, 5648 (1993).

23. Stephens P., Devlin F., Chabalowski C., M. J. Frisch. Ab Initio Calculation of Vibrational Absorption and Circular Dichroism Spectra Using Density Functional Force Fields, *J. Chem. Phys.,* **98**, 11623 (1994).

24. Lee C., Yang W., Parr R. G., Development of the Colle-Salvetti correlation-energy formula into a functional of the electron density, *Phys. Rev. B,* **37**, 785 (1988).

25. Weigend F., Ahlrichs R., Balanced basis sets of split valence, triple zeta valence and quadruple zeta valence quality for H to Rn: Design and assessment of accuracy, *P.C.C.P.,* **7**, 3297 (2005).

26. Schäfer A., Huber C., Ahlrichs R., Fully optimized contracted Gaussian basis sets of triple zeta valence quality for atoms Li to Kr, *J.Chem. Phys.,* **100**, 5829 (1994).

27. Wolinski K., Hinton J. F., Pulay P., Efficient implementation of the gauge-independent atomic orbital method for NMR chemical shift calculations, *J. Am. Chem. Soc.,* **112**, 8251 (1990).

28. Ditchfield R., Hehre W. J., Pople J. A., Self□Consistent Molecular□Orbital Methods. IX. An Extended Gaussian□Type Basis for Molecular□Orbital Studies of Organic Molecules, *J. Chem. Phys.,* 54, 724 (1971).

29. Rajan A., Strano M. S., Heller D. A., Hertel T., Schulten K., Length-Dependent Optical Effects in Single Walled Carbon Nanotubes†, *J. Phys. Chem. B.,* **112**, 6211 (2008).

30. Reed A. E., Weinhold F., Natural bond orbital analysis of near□Hartree–Fock water dimer, *J. Chem. Phys.,* **78**, 4066 (1983).

31. Refaely-Abramson S., Baer R., Kronik L., Fundamental and excitation gaps in molecules of relevance for organic photovolatics from an optimally tuned range-separated hyprid funtional, *Phys. Rev. B.*, **84**, 075144 (2011).

32. Pearson R. G., Absolute electronegativity and hardness correlated with molecular orbital theory, *Proceedings of the National Academy of Sciences.,* **83**, 8440 (1986).

33. Chandra A. K., Uchimaru T., Hardness Profile: A Critical Study, *J. Phys. Chem. A.,* **105**, 3578 (2001).

34. Calu L., Badea M., Chifiriuc M. C., Bleotu C., David G.-I., Ioniţă G., Măruţescu L., Lazăr V., Stanică N., Soponaru I., Synthesis, spectral, thermal, magnetic and biological characterization of Co(II), Ni(II), Cu(II) and Zn(II) complexes with a Schiff base bearing a 1,2,4-triazole pharmacophore, *J. Therm. Anal. Calorim.,* **120**, 375-386 (2015).

35. Dennington R., Keith T., J. Millam., GaussView, Version 5.0.8. Semichem Inc.: Shawnee Mission, KS. (2009).

36. Bauernschmitt R., Ahlrichs R., Treatment of electronic excitations within the adiabatic approximation of time dependent density functional theory, *Chemical Physics Letters.,* **256**, 454-464 (1996).

37. Casida M. E., Jamorski C., Casida K. C., Salahub D. R., Molecular excitation energies to high-lying bound states from time-dependent density-functional response theory: Characterization and correction of the time-dependent local density approximation ionization threshold, *J. Chem. Phys.,* **108**, 4439 (1998).

38. Van Caillie C., Amos R. D., Geometric derivatives of excitation energies using SCF and DFT, *Chem. Phys. Lett.,* **308**, 249 (1999).

39. Van Caillie C., Amos R. D., Geometric derivatives of density functional theory excitation energies using gradient-corrected functionals, *Chem.Phys. Lett.,* **317**, 159-164 (2000).

40. Furche F., Ahlrichs R., Adiabatic time-dependent density functional methods for excited state properties*, J. Chem. Phys.,* **117**, 7433 (2002).

41. Scharber M. C., Mühlbacher D., Koppe M., Denk P., Waldauf C., Heeger A. J., Brabec C. J., Design Rules for Donors in Bulk-Heterojunction Solar Cells—Towards 10% Energy-Conversion Efficiency, *J. Adv. Mater.,* **18**, 789-794 (2006).

42. Kumasaki M., Sasahara K., Nakajima Y., Thermal sensitivities of triazole derivatives and dinitrobenzene mixtures from the perspective of charge transfer, *J. Therm. Anal. Calorim.,* **125**, 331 (2016).

43. Xu A., Wang J., Wang H., Effects of anionic structure and lithium salts addition on the dissolution of cellulose in 1-butyl-3-methylimidazolium-based ionic liquid solvent systems, *Green. Chem.,* **12**, 268 (2010).

44. Youle R. J., Strasser A., The BCL-2 protein family: opposing activities that mediate cell death, *Nature reviews Molecular Cell Biology,* **9**, 47-59 (2008).

45. Yang P. H., Recent developments in the heterocyclic ketene aminal-based synthesis of heterocycles, *Res. Chem. Intermed.;* **42**, 5617 (2016).

46. Sundaraganesan N., Kalaichelvan S., Meganathan C., Joshua B. D., Cornard J., FT-IR, FT-Raman spectra and ab initio HF and DFT calculations of 4-N, N′-dimethylamino pyridine. *Spectrochim.*

Acta. Part. A., **71**, 898-906 (2008).

47. Swaminathan J., Ramalingam M., Sundaraganesan N., Molecular structure and vibrational spectra of 3-amino-5-hydroxypyrazole by density functional method, *Spectrochim. Acta. Part. A.,* **71**, 1776-1782 (2009).

48. Zayed E. M., Zayed M., Hindy A. M., Thermal and spectroscopic investigation of novel Schiff base, its metal complexes, and their biological activities, *J. Therm. Anal. Calorim.,* **116**, 391 (2014).

49. Solis F. J., Wets R. J.-B., Minimization by Random Search Techniques, *Mathematics of Operations Research.,* **6**, 19-30 (1981).

50. Zayed E. M., Zayed M., El-Desawy M., reparation and structure investigation of novel Schiff bases using spectroscopic, thermal analyses and molecular orbital calculations and studying their biological activities, *Spectrochim. Acta. Part. A.,* **134**, 155-164 (2015).

51. Mohamed G. G., Zayed E. M., Hindy A. M., oordination behavior of new bis Schiff base ligand derived from 2-furan carboxaldehyde and propane-1,3-diamine. Spectroscopic, thermal, anticancer and antibacterial activity studies, *Spectrochim. Acta. Part. A.,* **145**, 76-84 (2015).

52. Dametto P., Ambrozini B., Caires F., Franzini V., Ionashiro M., Synthesis, characterization and thermal behaviour of solid-state compounds of folates with some bivalent transition metals ions, *J. Therm. Anal. Calorim.,* **115**, 161-166 (2014).

53. Zayed E. M., Zayed M., Synthesis of novel Schiff's bases of highly potential biological activities and their structure investigation, *Spectrochim. Acta. Part. A.,* **143**, 81-90 (2015).

54. Han B., Li Z., Li C., Pobelov I., Su G., Aguilar-Sanchez R., T. Wandlowski. From self-assembly to charge transport with single molecules–an electrochemical approach. *Templates in Chemistry III: Springer.,* 181(2008).

55. Bharti A., Bharati P., Bharty M., Dani R., Singh S., Singh N., Mononuclear Ag(I), dinuclear and polymeric Hg(II) complexes of 3-mercapto-4-methyl-4H-1,2,4-triazole: Syntheses, spectral, X-ray, photoluminescence and thermal analysis, *Polyhedron*., **54**, 131-139 (2013).

56. Gruzdev M., Chervonova U., Zharnikova N., Kolker A., Mesomorphic azomethine complexes of Iron(III) based on 4,4′-dodecyloxybenzoyloxybenzoyl-4-salicylidene-2-aminopyridine, *Liq. Cryst.,* **40**, 1541-1549 (2013).

57. Ermolaev A., Smolentsev A., Mironov Y. V., Polymers based on anionic octahedral cluster chalcocyanohydroxorhenium complexes and cations $[Cu(En)_2]^{2+}$, Russ. *J. Coord. Chem.,* **40**, 558-564 (2014).

التحضير والتوصيف الهيكلي والسلوك الحراري والنشاط المضاد للميكروبات لكلا من النحاس والكادميوم والزنك في ترايزول ثيول ليجند بالمقارنة مع الحسابات المدارية الجزيئية النظرية

هيام عبدالرحمن عبدالسلام¹، ايهاب مصطفي زايد¹، محمد زايد² و محمود نعمان³

¹قسم الكيمياء الخضراء- شعبة بحوث الصناعات الكيماويه - المركز القومي للبحوث - الدقي - الجيزه - مصر.

²قسم الكيمياء - كلية العلوم - جامعة القاهره - الجيزه - مصر.

³قسم الرياضيات - كلية العلوم - جامعة القاهره - الجيزه - مصر.

تمت دراسة الخواص التركيبية والجزيئية للتريازول - الثيول تجاه أيونات المعادن الانتقالية وهي النحاس والكادميوم والزنك من خلال التحليلات الأولية والقياسات المغناطيسية والإلكترونية والتحليلات الحرارية .كما تم تقييم تفسير جميع مراحل التحلل الحراري. وتم تنفيذ جميع الحسابات باستخدام حزمة برامج Gaussian 09W

تم ربط الأطياف النظرية والعملية لكل من الليجند وخلباته المعدنية ووجد أنها تؤكد بعضها البعض.وبدراسة النشاط المضاد للميكروبات لليجند وخلباته المعدنية ضد بكتريا إيجابية الجرام وسلبية الجرام ونوعين من الفطر تبين انه ذات فاعليه جيده افضل من المضاد الحيوي المستخدم .